Article

Massive crustal carbon mobilization and emission driven by India underthrusting Asia

Check for updates

Wei Liu[1,2], Maoliang Zhang [1] ✉, Yi Liu[1], Lifeng Cui[1], Yuji Sano [3,4], Xiaocheng Zhou[5], Ying Li[5], Lihong Zhang[6], Yun-Chao Lang[1], Cong-Qiang Liu [1] & Sheng Xu [1] ✉

The active Himalayan-Tibetan orogen, where India underthrusts into Asia, is an important geological source of carbon dioxide (CO_2) emission into Earth's atmosphere. However, the extent to which Indian underthrusting could stimulate the mobilization of deeply-sourced carbon and its subsequent emission remains unknown. Here, we use a combination of field observations coupled with in-situ CO_2 flux measurements and helium and carbon isotopic data, to study the controls on CO_2 origins and fluxes in a 400-kilometre-long rift transecting northern Himalaya and southern Tibet. High diffuse CO_2 fluxes sustained by pure crustal fluids are confined to rift segments in the northern Himalaya, while toward southern Tibet, CO_2 fluxes become lower but mantle fluid inputs are identified. Such rift-related CO_2 degassing profile suggests metamorphic decarbonation and release of carbon-bearing fluids enhanced by the underthrusting Indian lower crust, agreeing well with Himalayan metamorphism and orogen-parallel lithospheric extension. Deep CO_2 fluxes from extensional tectonics in northern Himalaya and southern Tibet, primarily of crustal origins, are comparable to mantle CO_2 fluxes from global mid-ocean ridges. Our findings demonstrate that geophysical and geo-tectonic responses to continental underthrusting could facilitate massive crustal carbon mobilization and emission, making active collisional orogens globally important carbon sources.

The continental collision between India and Asia built up the Tibetan Plateau[1] that is essential for global carbon cycle and climate changes in the Cenozoic[2,3]. Over the past few decades, the Tibetan Plateau and its surrounding tectonically uplifted regions have been well documented for their role as atmospheric CO_2 sinks through silicate weathering and organic carbon burial in the geological past[3,4] and the global warming era at present[5,6]. Conversely, the Himalayan-Tibetan orogen is also considered as important CO_2 sources due to solid Earth (referring to the mantle and crust) carbon emissions by multi-stage magmatism[2], regional metamorphism[7], and enhanced erosion[8] driven by the India-Asia collision. As a result of ongoing magmatism and metamorphic decarbonation, deep CO_2 emissions are pervasive in modern volcanically and tectonically active regions of the Tibetan Plateau and its surroundings[9–14]. The co-existence of CO_2 removal from and emission into Earth's atmosphere has boosted a long-lasting debate on the net carbon budget of the Himalayan-Tibetan orogen[15]. Particularly, the heterogeneous deep CO_2 emissions at regional to global scales[16]

and spatially variable atmospheric CO_2 consumption rates[4] could cause large uncertainties in whole-Earth carbon cycling models that incorporate the Himalayan-Tibetan orogen as key end-members for the feedbacks between carbon sources and sinks[17,18].

With respect to the role of the India-Asia collision zone as a potential deep carbon source, reducing the uncertainties in CO_2 emission rates remains challenging due to the impracticality of carrying out field-based observations in the entire Himalayan-Tibetan orogen, which is the largest one on Earth at present. Nevertheless, clarifying spatial variations in CO_2 origins and fluxes across the India-Asia collisional orogen, as well as the controlling factors, would shed light on the variability of deep CO_2 emissions in response to continental collision dynamics. Northward underthrusting of India beneath Asia has exerted remarkable impacts on lithospheric structure[19], thermal state[20], rheological behavior[21], and active tectonics[22] of the Himalayan-Tibetan orogen, where the crustal thickness reaches approximately double that of normal continental crust[23]. These

[1]Institute of Surface-Earth System Science, School of Earth System Science, Tianjin University, Tianjin, China. [2]College of Resources and Environmental Engineering, Inner Mongolia University of Technology, Hohhot, China. [3]Marine Core Research Institute, Kochi University, Kochi, Japan. [4]Atmosphere and Ocean Research Institute, The University of Tokyo, Chiba, Japan. [5]Institute of Earthquake Forecasting, China Earthquake Administration, Beijing, China. [6]School of Geology and Geomatics, Tianjin Chengjian University, Tianjin, China. ✉e-mail: mzhang@tju.edu.cn; sheng.xu@tju.edu.cn

1

geophysical and geo-tectonic responses to Indian underthrusting are expected to play a fundamental role in the mobilization of carbon from its source, as well as the uprising and degassing of CO_2-bearing fluids en route to the surface. To elucidate the contribution of Indian continental underthrusting to deep carbon mobilization and emission, it is pivotal to establish a south-to-north CO_2 degassing profile (i.e., following the direction of India-Asia convergence) by linking surface observations of CO_2 emissions (e.g., gas geochemistry and outgassing fluxes) to origins of CO_2-bearing fluids at depth. However, previous studies on CO_2 degassing from active fault zones[11–13] are limited in space, and an across-orogen profile of the CO_2 origins and fluxes is yet to be constrained. Furthermore, the potential control of India-Asia collision on regional CO_2 emission variabilities, if any, remains untested. To our knowledge, the tectonic CO_2 degassing in the Himalayan-Tibetan orogen has rarely been interpreted from the causal effects of Indian underthrusting that could well reconcile geochemically constrained CO_2 origins and field-based observations of CO_2 fluxes.

Here, we quantitatively constrained the CO_2 origins and fluxes of the Tingri-Tangra Yumco rift (TTYR) in the central part of the India-Asia collision zone, extending approximately 400 km from northern Himalaya to southern Tibet (referring to the Tethyan Himalaya and Lhasa Block, respectively; Fig. 1a). We established a rift-related CO_2 degassing profile along the TTYR (Fig. 1b) based on (i) CO_2 origins constrained by $\delta^{13}C$-CO_2, $^3He/^4He$, and $CO_2/^3He$ of hydrothermal gases, and (ii) field-based measurements of diffuse soil CO_2 fluxes in hydrothermal fields, fault zones, and background areas ("Methods" section). Integrating the analysis of CO_2 origins and fluxes in the TTYR enables us to unravel how Indian underthrusting could facilitate carbon mobilization and emission through extensional tectonics in collisional orogens. By examining the spatial variations in CO_2 origins and fluxes from northern Himalaya to southern Tibet, possible controlling factors associated with Indian underthrusting (e.g., collision-zone geometry, crustal thermal structure, and lithospheric extension) were explored for the rift-related CO_2 degassing profile. Moreover, we
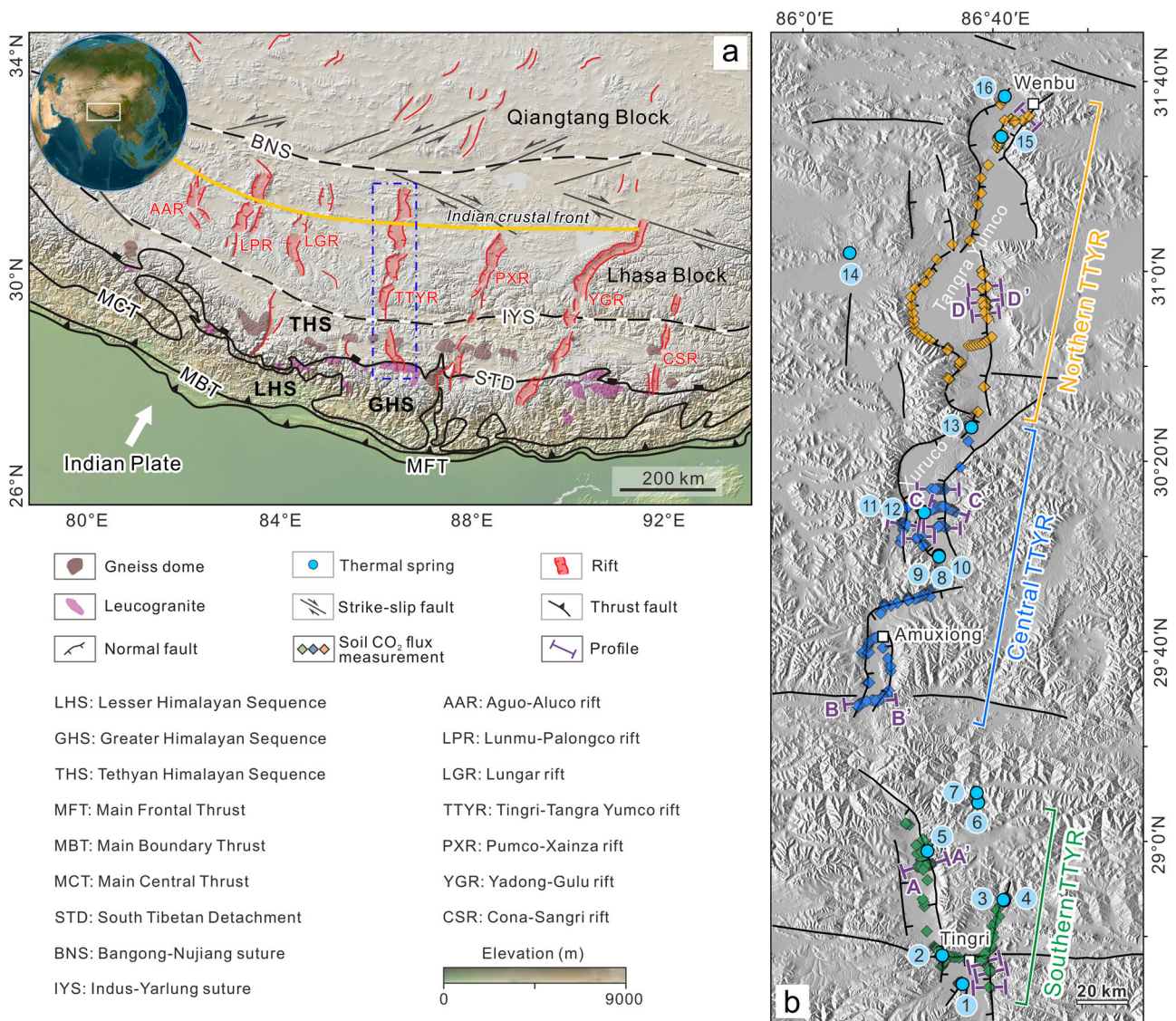

Fig. 1 | Tectonic framework of the Himalayas and southern Tibet, CO_2 flux measurements, and sample distribution in the study area. a Map of the Himalayan-Tibetan orogen showing major tectonic boundaries and extensional rift systems. Base map was created with GeoMapApp (www.geomapapp.org)/CC BY, and the hemisphere inset was generated using ArcGIS Earth software. Localities of the Himalayan domes and leucogranites are after ref. 51. The dash-dotted blue box shows the location of the TTYR. The yellow line represents the seismically inferred northern extent of the Indian crustal front[19]. **b** Distribution of CO_2 flux measurements and thermal springs in the southern, central, and north segments of the TTYR. Profiles AA′, BB′, CC′, and DD′ represent soil CO_2 measurements across active fault zones, as shown in Supplementary Fig. 8. The base map is from a 30-meter SRTM digital elevation model (www.earthexplorer.usgs.gov). Numbers represent hydrothermal fields from which bubbling gas samples were collected for geochemical analysis, with carbon and helium isotope data shown in Fig. 3a, b.

estimated the deep CO_2 output of extensional tectonics (i.e., rifts and normal faults) in the northern Himalaya and southern Tibet based on carbon isotope mass balance model and flux extrapolation ("Methods" section and Supplementary Information). Taking into account the CO_2 origins and fluxes across the India-Asia collisional orogen, we suggest that the geophysical and geo-tectonic responses to Indian underthrusting are the first-order controls on mobilization and emission of massive crustal carbon, making the Himalayan-Tibetan orogen a globally important carbon source.

Results and discussion
Carbon origins and secondary hydrothermal processes
The origin and evolution of CO_2-bearing fluids in hydrothermal systems are controlled by a series of physico-chemical processes[24–28], such as partial melting of the mantle or crustal source rocks, metamorphic decarbonation reactions, gas-water-rock interaction, calcite precipitation, and multi-component mixing. Particularly, the intricate secondary hydrothermal processes, which could result in He-CO_2 elemental and isotopic fractionation as reflected by δ^{13}C-CO_2 and CO_2/^{3}He data[24,29], indicate the need for caution when attempting to trace the origins of CO_2-bearing fluids using He-CO_2 systematics. For example, the CO_2/^{3}He ratios of the TTYR samples vary from 8.7×10^8 to 9.6×10^{12} and appear to decrease from south to north (Supplementary Fig. 1). However, it would be misleading to infer a south-to-north transition from mantle carbon sources to crustal carbon sources simply by comparing CO_2/^{3}He of samples with reference values of the crustal and mantle end-members[30,31]. Instead, hydrothermal degassing is more likely to result in preferential loss of He relative to CO_2 from the residual fluids (Supplementary Fig. 2). It should be noted that the relative lower CO_2/^{3}He and negative δ^{13}C-CO_2 values of several samples were likely modified by calcite precipitation and/or CO_2 partial dissolution in groundwater (Fig. 2), as supported by the presence of travertine deposits around the spring mouths and the higher solubility of CO_2 relative to He in the groundwater[24] (Fig. 2).

To further evaluate the influence of secondary hydrothermal processes, we modeled the trends of (i) calcite precipitation at 125 °C and 192 °C
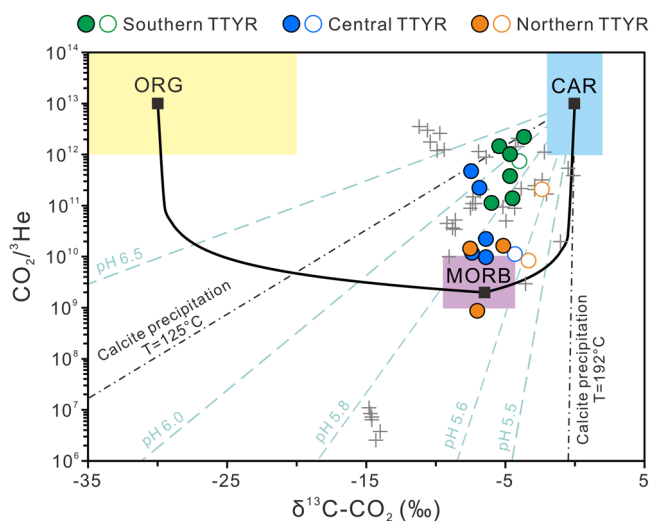

Fig. 2 | Plot of CO_2/^{3}He versus δ^{13}C-CO_2 for hydrothermal gases. The mixing lines between mantle (MORB), organic sediment (ORG), and carbonate (CAR) end-members are shown for comparison. Filled and open symbols represent data in this study and literature data, respectively. Data from the Yadong-Gulu rift (YGR) are shown by gray crosses. Black dotted lines represent predicted calcite fractionation model trends for CO_2 loss by calcite precipitation at 125 °C and 192 °C (after ref. 26). Light blue dashed lines show the predicted trends for gas dissolution over a range of pH values at 50 °C (average temperature of the studied thermal springs) (after ref. 25). Assuming a starting carbonate-like δ^{13}C value is 0.3‰ for metamorphic CO_2 and CO_2/^{3}He = 1×10^{13} in the predicted model lines for calcite precipitation and partial gas dissolution (after ref. 44).

following Barry et al.[26] and (ii) CO_2 dissolution during gas-water interaction over a range of pH values (5.5–6.5) at a fixed temperature of ~50 °C (i.e., average sample temperature measured in the field) following Gilfillan et al.[25] (Fig. 2). The selection of temperature for calcite precipitation modeling is supported by reservoir temperature (average = 146 °C; ref. 32) of the TTYR thermal springs. Considering that the Himalayan-Tibetan orogen is characterized by a remarkably thick crust (thickness up to 70 km[19]) and abundant carbon-bearing metamorphic rocks and sedimentary rocks[12,33], the carbonate/metamorphic end-member was chosen as the starting point for calcite fractionation and CO_2 dissolution models (Fig. 2). This is consistent with the He-C isotopic data and mixing calculations that show predominant origins of the CO_2-bearing fluids from a crustal carbonate/metamorphic end-member (see details below). The modeled lines agree well with the dataset and the hydrothermal gases may have been affected by calcite precipitation and/or CO_2 dissolution to different degrees (Fig. 2). Notably, it should be clarified that the role of secondary processes deduced from the modeling is inevitably simplified for the complex migration paths of hydrothermal fluids through the thick crust of the Himalayan-Tibetan orogen.

Although secondary hydrothermal processes occurred and may have modified chemical and isotopic compositions of the CO_2-bearing fluids[24] (i.e., masking their true source), we note that most samples are within the envelope area defined by the MORB, CAR, and ORG end-members (Fig. 2), which represents the expected results of the ternary mixing model proposed by Sano and Marty (ref. 31). This may suggest limited impacts of secondary hydrothermal processes on the chemical and isotopic composition of the CO_2-bearing fluids (i.e., limited He-CO_2 fractionation) for most samples, and this possibility requires further assessment. Based on the above assumption, we calculated the proportions of different carbon source components (i.e., mantle, carbonate rocks, and organic sediments) following a ternary mixing model[31] (Fig. 2) as expressed by the equations below:

$$(^{13}C/^{12}C)_{Obs} = f_{MORB} \times (^{13}C/^{12}C)_{MORB} + f_{CAR} \times (^{13}C/^{12}C)_{CAR} + f_{ORG} \times (^{13}C/^{12}C)_{ORG} \quad (1)$$

$$1/(^{12}C/^3He)_{Obs} = f_{MORB}/(^{12}C/^3He)_{MORB} + f_{CAR}/(^{12}C/^3He)_{CAR} + f_{ORG}/(^{12}C/^3He)_{ORG} \quad (2)$$

$$f_{MORB} + f_{CAR} + f_{ORG} = 1 \quad (3)$$

where subscripts Obs, MORB, CAR, and ORG refer to the observed value of the sample, mantle, carbonate rocks, and organic sediments, respectively. Reference values for the MORB, CAR, and ORG end-members are as those in Sano and Marty (ref. 31), which are: δ^{13}C = -6.5 ± 2.5‰ and CO_2/^{3}He = 2×10^9 for MORB-type mantle, δ^{13}C = 0 ± 2‰ and CO_2/^{3}He = 10^{13} for CAR, and δ^{13}C = -30 ± 10‰ and CO_2/^{3}He = 10^{13} for ORG.

The results show that three samples (21CZX1-1, 21CZX2-3, and 21CZX3-2 from the Chazi hydrothermal field) may have been remarkably affected by secondary processes because of their low CO_2/^{3}He ratios and abnormally high proportion of mantle carbon inputs (Supplementary Data 1); the latter is at odds with the pure crustal fluid sources evidenced by He isotope data (see details below). It is evident that the crustal carbon components are dominant in the entire TTYR; and if not considering the Chazi samples, the southern and central TTYR would be characterized by >99% crustal carbon contributions, while remarkable mantle carbon inputs (12–14%) are found in the northern TTYR (Supplementary Data 1). We speculate a pure crustal (metamorphic) carbon source for the southern and central TTYR and a crust-dominated (but showing clear mantle inputs) carbon source for the northern TTYR. Notably, the relative proportion of mantle carbon and crustal metamorphic carbon in the deeply-sourced carbon end-member is challenging to be quantitatively constrained due to the difficulty in distinguishing between metamorphic carbon and shallow carbon (e.g., carbonate dissolution and organic matter

decomposition) solely based on the ternary mixing model (Fig. 2). In addition, considering the fraction of the original carbon removed by secondary processes during the upward migration of deeply-sourced CO_2-bearing fluids, it is plausible that our observations of deep CO_2 fluxes at the surface only represent part of the original amount of carbon (e.g., CO_2) below the study area.

Rift-related hydrothermal degassing profile from northern Himalaya to southern Tibet

Following the Indian motion to the north, we compared the $\delta^{13}C$-CO_2 and $^3He/^4He$ values of hydrothermal gases (Figs. 3a and 3b) and average soil CO_2 fluxes of hydrothermal fields (Fig. 3c) relative to the distance from the Main Frontal Thrust (MFT), which represents the southernmost boundary

Fig. 3 | Carbon and helium isotopes of hydrothermal gas samples, average soil CO_2 fluxes, geophysically imaged collision-zone structure, and geological profile across the Himalayas and southern Tibet. Abbreviations are as in Fig. 1. Filled and open symbols in Panels **a** and **b** represent data in this study and literature, respectively. **a** Plot of $\delta^{13}C$-CO_2 values versus latitude of sampling sites for hydrothermal gases. **b** Plot of $^3He/^4He$ (R_C/R_A) versus latitude of sampling sites for hydrothermal gases. Samples from the YGR[11,12,35,38] and MCT (see ref. 38. and references therein) are shown for comparison (see compiled data in Supplementary Data 2). **c** Average soil CO_2 flux (g m^{-2} d^{-1}) versus latitude of the hydrothermal fields. The compiled soil CO_2 flux data of hydrothermal fields in the Himalayas and southern Tibet are summarized in Supplementary Table 1. Note that the results of soil CO_2 fluxes in fault zone profiles and background areas investigated in this study are not shown in Panel **c**. **d** Receiver function image[19] showing seismic velocity profile across the Himalayas and southern Tibet. Panel **d** refers to Panel **e** and provides seismic evidence for collision-zone structure from crustal to mantle depths. Note that there are no corresponding relationships between Panel **d** and Panels **a**, **b**, and **c**. **e**, Geological interpretation of the India-Asia collision-zone structure (modified from ref. 19). Main Himalayan Thrust (MHT) represents the lower boundary of the Himalayan orogenic wedge. The dashed purple lines show eclogitization of the horizontal portion of the underthrusting Indian lower crust. A broad layer of LVZs (low-velocity zones) in the Himalayas and southern Tibet is shown by the areas of dashed green lines and black triangles above the underthrusting India. Shallow LVZs are scattered in the upper crust. The light blue band in Panels **a**–**c** represents the Indian crustal front constrained by the 31°N discontinuity[19].
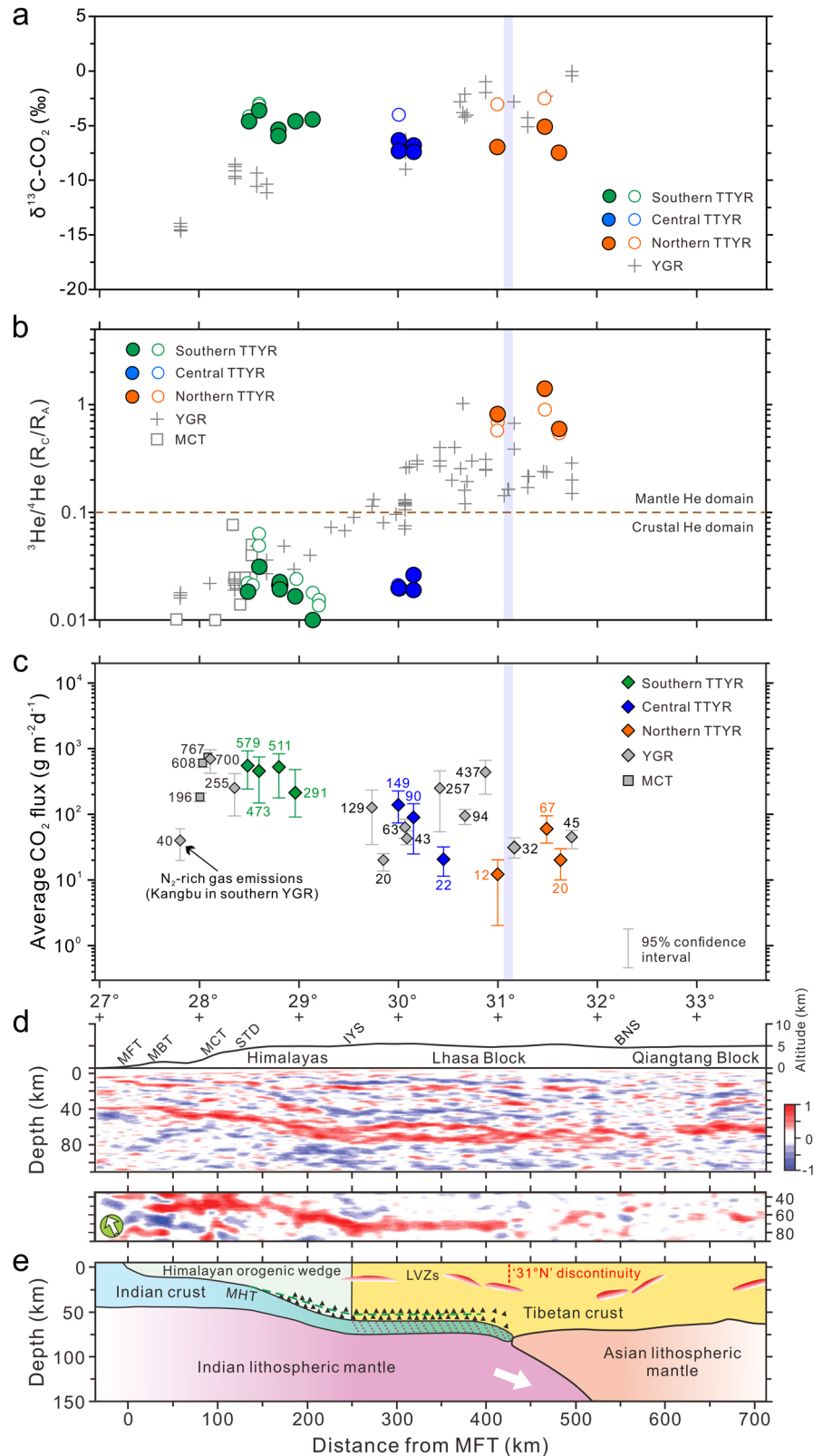
recording the India-Asia collision. This comparison defines a rift-related hydrothermal degassing profile in terms of C-He isotopes and diffuse CO_2 emissions from northern Himalaya to southern Tibet. Unlike the relatively wide $\delta^{13}C\text{-}CO_2$ range (–14.8 to +0.2‰; refs. 11,34,35) observed in the Yadong-Gulu rift (YGR; Fig. 1a), the TTYR samples have a much narrower range of $\delta^{13}C\text{-}CO_2$ values (–7.5 to –2.6‰; Fig. 3a). Spatially, there are almost no variations in $\delta^{13}C\text{-}CO_2$ among southern, central, and northern segments of the TTYR, which differs from a northward-increasing trend in $\delta^{13}C\text{-}CO_2$ along the YGR[12]. The $\delta^{13}C\text{-}CO_2$ data could be influenced by multiple factors that may contribute to the origin and transport of CO_2-bearing fluids, such as mantle carbon inputs, crustal lithology (e.g., limestone vs. meta-sedimentary rocks), addition of biogenic carbon into the hydrothermal fluids, and solubility-controlled phase separation (e.g., hydrothermal degassing and calcite precipitation). As for the majority of the TTYR samples that show limited influence by He-CO_2 elemental and isotopic fractionation (Fig. 2), we find that the southern and central TTYR are characterized by a pure crustal carbon source (mantle carbon <1%), while mantle carbon inputs (12–14%) are remarkable in the northern TTYR. This is consistent with the relative proportions of the crustal and mantle fluids calculated from He isotope systematics of the hydrothermal gases (Supplementary Data 1), as detailed below.

Since (i) CO_2 is believed to be a primary carrier for He migration through the crust[30] and (ii) He is chemically inert and is a powerful tracer for quantitatively constraining the inputs of mantle and crustal fluids, the origins of CO_2-bearing fluids can be interpreted from air-corrected $^3He/^4He$ data (R_C/R_A, where R_A = air $^3He/^4He$ = 1.39×10^{-6}). We note that a first-order feature of the rift-related hydrothermal degassing profile is the contrasting He source components among different rift segments (Fig. 3b). Specifically, a pure crustal domain of He sources dominates the southern and central TTYR ($^3He/^4He$ = 0.01–0.06 R_A, corresponding to null or <1% mantle He inputs), whereas in the northern TTYR, the proportion of mantle fluids in the CO_2-bearing fluids could reach ~7–17% [$^3He/^4He$ = 0.55–1.41 R_A, well over the canonical crustal value of 0.02 R_A (ref. 36)]. The along-rift $^3He/^4He$ variations in the TTYR are consistent with previously identified patterns of $^3He/^4He$ distribution in the Himalayas and the hinterland Tibetan Plateau[37–39] (Fig. 3b; see also Supplementary Fig. 3). Moreover, to the south of the Himalayan crest, large amounts of crustal fluids ($^3He/^4He$ = 0.003–0.076 R_A; refs. 38,40) have also been observed in the Main Central Thrust (MCT), suggesting a pure crustal fluid source for hydrothermal systems in the Himalayan fold-and-thrust belt. In stark contrast, the near N-S striking extensional rifts that transect the northern Himalaya and southern Tibet (generally located to the north of the Himalayan crest; Fig. 1a) show a prominent transition in origins of CO_2-bearing fluids from a pure crustal domain in the south to a domain characterized by discernible northward-increasing inputs of mantle fluids (e.g., up to 7–17% in the northern TTYR; Fig. 3b). We suggest that such transition in fluid origins constrained by C-He elemental and isotopic systematics (Figs. 2 and 3b) may point to the impact of continental collision-related properties of the Himalayan-Tibetan orogen, such as crust-mantle structure[19] and crustal thermal state[20], on the mobilization of carbon in its sources from northern Himalaya to southern Tibet.

Figure 3c illustrates the variations in average soil CO_2 fluxes of hydrothermal fields from the Himalayas to southern Tibet (Supplementary Table 1). Clearly, the southern TTYR exhibits higher average soil CO_2 fluxes (291–579 g m^{-2} d^{-1}) than observed in the central and northern TTYR (12–149 g m^{-2} d^{-1}) (Supplementary Fig. 4). Except for one hydrothermal field dominated by N_2-rich gas emissions (i.e., Kangbu in southern YGR[12]; Fig. 3c), the available data of soil CO_2 fluxes show that the Himalayas are currently experiencing vigorous degassing of CO_2-bearing fluids [e.g., 196–767 g m^{-2} d^{-1} in the MCT[10], 255–700 g m^{-2} d^{-1} in southern YGR[12], and 291–579 g m^{-2} d^{-1} in the TTYR (this study)], as expected in the global-scale tectonic CO_2 degassing model[16]. To the north of the Indus-Yarlung suture (Fig. 1a), most hydrothermal fields ($n = 13$) in the TTYR and YGR have lower average soil CO_2 fluxes (12–149 g m^{-2} d^{-1}) than observed in the Himalayas (Fig. 3c). Two localities showing high soil CO_2 fluxes (253 and

437 g m^{-2} d^{-1}, respectively) in the northern YGR[11] may result from localized high influx of CO_2-rich fluids. If only considering hydrothermal fields with CO_2-rich gas emissions, the average diffuse soil CO_2 fluxes would generally exhibit a good correlation with latitude [R^2 = 0.528, p < 0.001 ($n = 22$); Supplementary Fig. 5], suggesting spatially variable controls on CO_2 degassing from the Himalayas to southern Tibet.

Taking CO_2 origins and fluxes together, we find that high CO_2 fluxes are sustained by pure crustal fluids in the Himalayan orogenic wedge, a wedge-shaped portion above the underthrusting Indian lower crust (Fig. 3d, e), while relatively lower CO_2 fluxes dominate rift segments in southern Tibet where mantle carbon inputs are discernible (Fig. 3b, c). Notably, tectonic CO_2 emissions from the Himalayan-Tibetan orogen are generally dominated by crustal decarbonation. Furthermore, it is striking that the geophysically imaged geometry of the orogenic crust (Fig. 3d, e; ref. 19) corresponds well with variations in CO_2 origins and fluxes from the Himalayas to southern Tibet. As observed in the TTYR, pure crustal carbon sources are generally identified in regions above the underthrusting Indian lower crust, although it remains uncertain whether mantle carbon inputs have occurred in the gap zone between the central and northern TTYR [i.e., the rift segment approximately between 30°N and 31°N to the south of the Indian crustal front that is defined by the so-called "31°N discontinuity" (Fig. 3b); ref. 19]. But in the YGR, mantle fluid signals ($^3He/^4He$ > 0.1 R_A) were identified as far as ~110 km southward from the surface projection of the Indian crustal front[34,37,38], suggesting that mantle carbon inputs to hydrothermal systems may vary among the near N-S striking extensional rifts. A possible explanation for such rift-dependent carbon mobilization and emission mode could be the orogen-parallel changes in morphology (e.g., subduction angle) and collision-zone dynamics (e.g., tearing and/or break-off) of the subducting Indian plate[38,39,41], which have the potential to determine the distribution, amounts, and rates of mantle carbon supply to the extensional rifts in southern Tibet.

Carbon mobilization driven by Indian underthrusting

An intriguing feature of the rift-related CO_2 degassing profile lies in the crustal portion above the underthrusting Indian lower crust, which is bounded by the MFT to the south and the Indian crustal front to the north (Fig. 3e). Intensive mobilization of carbon is expected to occur at crustal levels beneath the Himalayan-Tibetan orogen, sustaining high CO_2 fluxes observed at the surface, particularly in the Himalayan orogenic wedge (Fig. 3c, e). This may suggest the fundamental role of Indian underthrusting in mobilization of crustal carbon from its sources. To address this possibility, we integrated plausible constraints from geophysics and geo-tectonics of the collision-zone crust that have close affinities with the underthrusting Indian continent (Fig. 4). Considering the absence of volcanic activities in southern Tibet for the past ca. 8 million years[1], and the non-volcanic nature of the Himalayan orogenic wedge over even longer timescales[42], the partial melting and intruded magmas as the reservoirs to feed CO_2 degassing are unlikely scenarios. Instead, the mobilization of carbon through metamorphic decarbonation has been widely invoked as a plausible mechanism for CO_2 origins in field-based and experimental studies on active orogenic degassing[9,12,33,43,44]. In this section, the controlling factors for metamorphic decarbonation are considered to explain the high CO_2 fluxes observed in the Himalayan orogenic wedge.

A primary feature of young and mature collisional orogenic systems, such as the Cenozoic Himalaya, is the evolution of crustal thermal structure during continental collision processes[45,46]. Currently, the active extensional rifts (mostly initiated at 13 ± 3 Ma[42]) in the northern Himalaya and southern Tibet have high surface heat flows (up to 100–300 mW m^{-2} as shown in Fig. 4a; refs. 21,47), consistent with the predictions in thermal structure model of continental collisional orogens[46]. In addition, thermal modeling results of the Indian underthrusting beneath Asia have suggested temperatures of ≤600 °C for the crust of the Himalayan orogenic wedge (Fig. 4b; ref. 20). Under such a crustal thermal structure, metamorphic decarbonation reactions could occur roughly within crustal depths of 10–25 km (>300 °C; ref. 48). Notably, the simulated geotherms become shallower to

Fig. 4 | Surface heat flows, earthquakes, thermal structure, and geological evidence for the massive crustal carbon mobilization and emission in the Himalayan orogenic wedge. a Surface heat flows and seismic frequency versus distance from MFT across the Himalayas and southern Tibet. Filled circles represent measured surface heat flows from the global heat flow database: update 2023 (www. ihfc-iugg.org). Earthquake events are from USGS. **b** Model of crustal thermal structure across the Himalayas and southern Tibet[20]. Contours are at 50 °C intervals. Blue lines denote the boundaries between the Tibetan crust, Indian crust, and the mantle based on seismic images of lithospheric structure[19]. **c** Geological profile across the Himalayan-Tibetan orogen showing outcropping of domes and leucogranites in the Himalayan orogenic wedge, especially the northern Himalaya (modified from ref. 51. **c**). Abbreviations are as in Fig. 1.
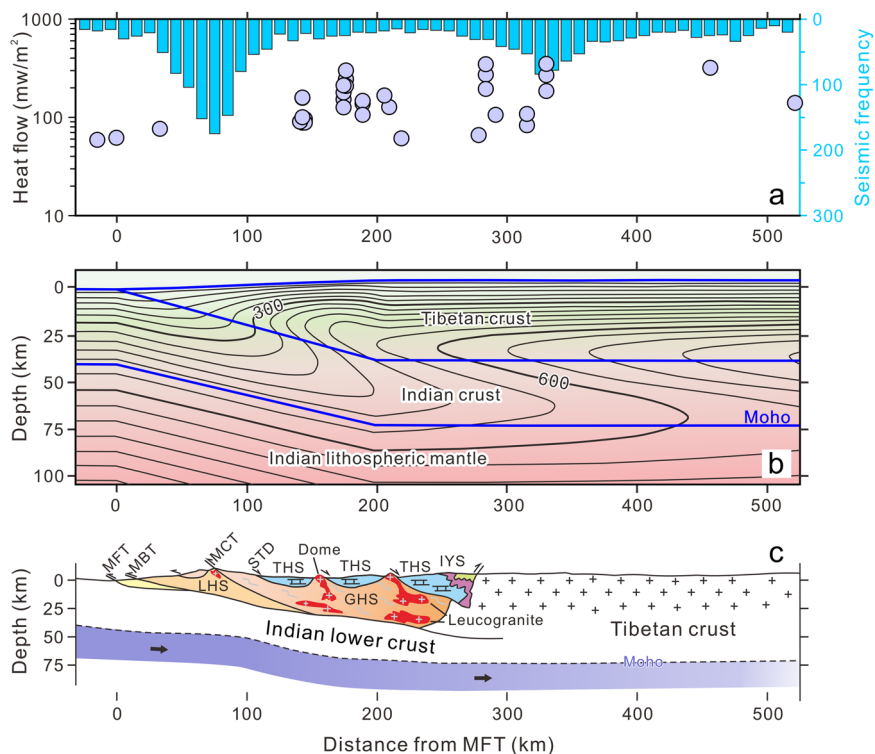
the surface in the regions approximately 100–200 km north of the MFT (Fig. 4b), which agrees well with the observed high CO_2 fluxes in the MCT and southern segments of the TTYR and YGR (Fig. 3c). We, therefore, suggest that metamorphic decarbonation reactions at crustal levels could be enhanced by warming (i.e., elevated geotherms[20,21]) of the Himalayan orogenic wedge during India-Asia continental collision (i.e., the underthrusting of India beneath Asia).

In accretionary wedges of collisional orogens, a thermally weakened infrastructure is likely to generate lateral crustal flows toward the orogenic foreland[45]. This is a widely accepted model for the Himalayas where geophysically imaged anomalies of low electric resistivity[49] and low seismic velocity[19] are plausible mid-crustal channel flow that migrates toward the Himalayan erosional front[23,50]. The channel flow probably represents hot and ductile materials (e.g., anatectic melts involved in the formation of Himalayan leucogranites[51]) that could promote crustal CO_2 production by heating the overlying carbon-bearing rocks (e.g., carbonate and calc-silicate rocks). Possible geological evidence for such heating-related metamorphic decarbonation could be the presence of the Himalayan leucogranites and gneiss domes in southern segments of the extensional rifts[42,50] (Fig. 4c), including the southern TTYR and southern YGR (Fig. 1a). Notably, geological evidence for metamorphism was not observed in the southern Tibet where CO_2 fluxes are low, suggesting that the Himalayan metamorphism is critical for crustal carbon mobilization. Besides the heating effects of mid-crustal channel flow, the infiltration of aqueous fluids could remarkably increase the efficiency of metamorphic decarbonation[52], which is a plausible scenario for the Himalayan orogenic wedge due to dehydration of the Indian lower crust above the inclined portion of the Main Himalayan Thrust (MHT; ref. 21).

Carbon emission facilitated by extensional tectonics

A global-scale carbon emission model[16] reveals that the Tibetan Plateau and its surroundings have a high probability of CO_2 degassing related to extensional tectonics, which is in comparable magnitude with the East African rift system that was suggested to have CO_2 outgassing flux of 71 ± 33 Mt yr^{-1} (ref. 53). Tectonically, the control of Indian underthrusting on deep CO_2 emissions from extensional rifts such as the TTYR could be

interpreted in models that the eclogitized Indian lower crust may have served as a dynamic trigger for the orogen-parallel lithospheric extension in the Himalayas and southern Tibet[22,54,55]. In the extensional regimes of rifts and normal faults[22], the CO_2-bearing fluids could migrate efficiently to the surface and thus sustain high CO_2 fluxes[16]. Due to the ongoing continental collision, earthquake events could promote the formation of highly permeable fracture networks in the brittle upper crust and facilitate efficient uprising and degassing of the CO_2-bearing fluids[10,56]. As shown in Fig. 4a, the spatial variations in the frequency of earthquake events, which mostly occurred in the Himalayan orogenic wedge, may suggest more favorable pathways for the upward migration of CO_2-bearing fluids in the Himalayas than in southern Tibet. Thermodynamic modeling results show that the fluid immiscibility in metamorphic C–O–H–salt fluids is crucial for driving the upward CO_2 transport from the deep crust of active orogens[33]. This process is particularly facilitated by earthquake-induced brittle fracturing of the crust. Overall, regional/contact metamorphism, crustal thermal state (e.g., geothermal gradients), and active structures (e.g., extensional tectonics) involved in source-to-surface transport of the mobilized crustal carbon through the extensional rift systems have close affinities with the underthrusting India, which could well reconcile geochemically constrained CO_2 origins and field-based observations of CO_2 fluxes.

Himalayan-Tibetan orogen as important carbon sources

We established the potential links between surface observations of active CO_2 degassing (i.e., origins and fluxes) and deep metamorphic decarbonation in the Himalayan-Tibetan orogen (Fig. 5). The combined geophysical and geo-tectonic responses to the Indian underthrusting, such as the collisional metamorphism that characterizes the Himalayan orogenic wedge[23,50], could stimulate massive crustal carbon mobilization. By efficient outgassing through rifts and normal faults[11,12], as well as in the Himalayan fold-and-thrust belt[9,43], the CO_2-rich fluids produced by metamorphic decarbonation reactions at crustal levels[33] represent remobilization of carbon that has been stored in crustal rocks over geological timescales.

Our estimation yielded a total CO_2 flux of 17.4 ± 4.1 Mt yr^{-1} for the TTYR, and by subtracting shallow carbon contributions, we obtained a deep CO_2 flux of 2.97 ± 1.01 Mt yr^{-1} (Supplementary Table 2). Notably, our

Fig. 5 | Conceptual model showing massive crustal carbon mobilization and emission driven by the underthrusting of India beneath Asia. Abbreviations are as in Fig. 1. The CO_2 emissions in southern and central TTYR are derived from metamorphic decarbonation at lower crustal and upper crustal depths, while those in the northern TTYR are supplied mainly by crustal fluids but show contributions from mantle fluids (up to 7–17%). The migration of mid-crustal channel flow toward the Himalayan erosional front is shown, which could be partially molten, serve as the heat source for the overlying carbon-bearing rocks (e.g., calc-silicate and marble) in the upper crust, and mobilize massive CO_2 from the crustal sources. The Himalayan gneiss domes and leucogranite plutons are shown as the geological evidence for the extension and melting of the Himalayan orogenic crust. The presence of CO_2 + H_2O fluids is expected for dehydration of the Indian lower crust above the inclined portion of the Main Himalayan Thrust[21], which is likely to facilitate the metamorphic decarbonation reactions.
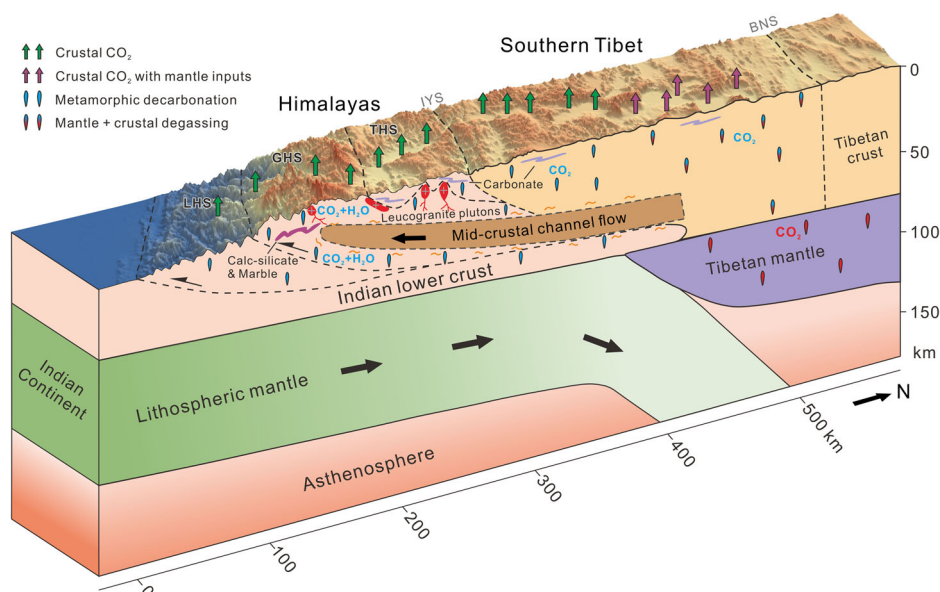
calculation methods only take into account the deep carbon fraction, which could yield conservative and relatively unbiased estimates of deep CO_2 fluxes for the Himalayan-Tibetan orogen. Further extrapolation of our estimates from the TTYR to seven major near N-S striking rifts and other smaller-scale normal faults in the northern Himalaya and southern Tibet gave rise to a total deep CO_2 output of 37 ± 21 Mt yr^{-1} (Methods and Supplementary Information). This estimate is comparable to mantle CO_2 fluxes from global mid-ocean ridges (MOR) if considering (i) recently reported MOR CO_2 fluxes of ~58 Mt yr^{-1} (ref. 57), and (ii) an updated mantle ^{3}He flux from MOR (527 ± 102 mol yr^{-1}; ref. 58) that corresponds to a mantle CO_2 flux of ~46 Mt yr^{-1}.

We emphasize that more work is required to reduce the scaling-up uncertainties in CO_2 flux estimation for large-scale active collisional orogens such as the Himalayas and Tibet. For example, water-gas interaction (e.g., partial exsolution and dissolution of gas in groundwater) and subsurface calcite precipitation could lead to underestimation of the deep CO_2 output at the surface[24,59,60] and need to be considered in future work. The effect of such secondary processes on CO_2 flux estimation is still challenging to be quantitatively constrained so far. Nevertheless, our up-to-date estimate of deep CO_2 emissions from extensional tectonics indicates that the Himalayan-Tibetan orogen is a globally important carbon source. Furthermore, the estimated deep CO_2 output is conservative because the rifts and normal fault systems in more northerly and easterly tectonic units (e.g., Qiangtang Block and Songpan-Ganzi Block) of the Tibetan Plateau were not included in our calculation (Methods). It is thus plausible that deep CO_2 output of the Himalayan-Tibetan orogen would be comparable in magnitude with the mantle CO_2 output from global MOR systems, even in case of comparison with the CO_2 flux estimate for the MOR (~97 Mt yr^{-1}) based on ^{3}He flux of 1000 ± 250 mol yr^{-1} and $CO_2/^3$He ratio of 2.2×10^9 (ref. 61).

Role of orogenic CO_2 emissions in global carbon cycle

By linking geochemically constrained CO_2 origins and field-based observations of CO_2 fluxes along a rift-related profile following the direction of Indian underthrusting, we demonstrate that geophysical and geo-tectonic processes in response to the underthrusting of India beneath Asia could stimulate the release of huge amounts of crustal carbon from Earth's largest active collisional orogen. Importantly, the outgassed CO_2 in the Himalayan-Tibetan orogen is primarily of crustal origins, with its total output ($\gg 37 \pm 21$ Mt yr^{-1}) in comparable magnitude with the mantle CO_2 fluxes (46–97 Mt yr^{-1}; Supplementary Fig. 6) from global MOR systems. We suggest that the massive crustal CO_2 emissions in tectonically active

collisional orogens must be considered equally important as the mantle CO_2 from MOR[57,58,61] and intra-continental settings such as the East African rift[53,62,63]. To thoroughly understand the framework of solid Earth degassing and carbon cycling feedbacks, an important theme of future work, tectonic CO_2 emissions from active collisional orogens should be combined with volcanic CO_2 outputs[64] (e.g., MOR[57] and subduction zones[60,65]) to give an unbiased average δ^{13}C value of deep carbon for the global carbon isotope mass balance model[66,67]. Our findings would provide new insights into how continental collision dynamics could influence the mobilization and emission of crustal carbon over an active orogen-wide scale, which is crucial to our understanding of solid Earth degassing and deep carbon cycling processes from a whole-Earth plate tectonic point of view.

Methods

A series of near N-S striking extensional rifts have developed in northern Himalaya and southern Tibet (Fig. 1a) as a result of orogen-parallel extension since Miocene time[22]. These rifts are roughly spaced by a distance of ~150–200 km and are large-scale focal zones of modern hydrothermal activities (hot and boiling springs, geysers, steam fissures, and fumaroles; refs. 11–13,34), as well as diffuse soil CO_2 emissions. Centering in the major seven rift systems, the TTYR consists of several kinematically linked rift segments, which could be divided into the southern, central, and northern TTYR (Fig. 1b). Our field campaign in the TTYR was conducted from May to July 2021, covering the entire rift from the northern Himalaya to southern Tibet, to quantify the CO_2 outgassing fluxes and decoding the origins of the CO_2-bearing fluids.

Sample collection and analysis

Temperature, pH, and electrical conductivity (EC) were measured for the main spring outlets of thermal springs in the field (Supplementary Data 1). Free gas samples ($n = 16$) from bubbling springs were collected into low-He diffusivity glass containers by water displacement method. Standard procedures of sample collection in the field and timely laboratory analysis after sampling were adopted to minimize air contamination. Soil gas samples ($n = 24$) were collected from depths of 20–90 cm in soils of the measurement sites for analysis of CO_2 concentrations and carbon isotopic compositions (Supplementary Fig. 7). Gas chemistry, He, and C isotope analysis were conducted at Oil and Gas Research Center, Northwest Institute of Eco-Environment and Resources, Chinese Academy of Sciences. Major gas components (such as CO_2, N_2, CH_4, O_2, and Ar) were determined using a MAT 271 mass spectrometer. About 1 mL of gas was extracted from the

sample bottle using a syringe and then injected into the sample entrance line connected to the mass spectrometer. Repeated analysis of air standard yields analytical error <2% for major gas species (N_2, O_2, Ar, and CO_2). Carbon isotopic compositions in CO_2 of thermal spring gases and soil gases were analyzed by Agilent 6890 gas chromatograph (GC) coupled to Thermo-Finnigan Delta Plus-XP Isotope Ratio Mass Spectrometer (IRMS). An analytical uncertainty of GC-IRMS is < ±0.3% based on repeat measurements of gas standards. Helium isotopes were determined by a Noblesse noble gas mass spectrometer equipped with a two-stage gas separation line and purification system. Before measurement by the mass spectrometer, the free gases (~500 μL) were purified by exposure to a spongy titanium furnace heated to 800 °C, removing most active gases (e.g., H_2O, O_2, N_2, and CO_2). H_2 in the gases was eliminated by a Zr-Al getter running at room temperature. Next, the purified noble gases were trapped by a cryogenic trap filled with activated charcoal. He and Ne were released into the mass spectrometer at a cryogenic trap temperature of 70 K. Then, ^{4}He, ^{20}Ne, and ^{22}Ne were examined with a Faraday collector, and ^{3}He and ^{21}Ne were analyzed with an electron multiplier. The stability of the Noblesse Mass Spectrometer was monitored by repeated analysis of standard air before and after analyzing the sample every day. The air collected from the top of Gaolan Mountain, South of Lanzhou City, was analyzed to meet laboratory standards during routine measurement. Repeated analysis of the standard air yields an analytical error of less than 1.5% for the ^{3}He/^{4}He value. The analytical data of bubbling gases from thermal springs are summarized in Supplementary Data 1. For comparison, gas geochemical data reported in the literature are compiled in Supplementary Data 2. In addition, volume fraction and carbon isotopic composition of CO_2 in soil gases are summarized in Supplementary Data 3.

Quantifying diffuse soil CO_2 emissions and uncertainty assessment

A total of 939 points of in-situ diffuse soil CO_2 fluxes (Supplementary Data 4) were obtained from the TTYR between May and July 2021, following the accumulation chamber method[68]. Specifically, soil CO_2 fluxes were measured by a West Systems LI820 infrared CO_2 detector with a CO_2 detection range of 0–2% and an accuracy of 4%. An open-bottomed accumulation chamber with a volume of 6.19×10^{-3} m^3 was placed directly on the soil surface to form a tight seal (Supplementary Fig. 7), and the CO_2 flux was calculated by the linear segment that represents the natural accumulation of CO_2 concentration with time in the chamber. To minimize the biological influence on accumulated CO_2 in the chamber, we selected measurement points in non-vegetation areas or removed the vegetation cover and the uppermost few centimeters of the soils. During our fieldwork, there was little precipitation in the TTYR, showing typical meteorological features in the Tibetan Plateau that are suitable for soil CO_2 flux measurements considering the influence of soil moisture on CO_2 outgassing via micro-seepage. To constrain the distribution and magnitude of CO_2 fluxes in the rift, we employed a sampling grid of 20–50 m in hydrothermal fields. For active faults, the measurement spacing was 50–500 m for observational profiles of soil CO_2 fluxes that are generally perpendicular to the fault strike (Fig. 1 and Supplementary Fig. 8). Moreover, in areas with less assessable topography and transportation limitations, the spacing between adjacent soil CO_2 profiles may extend up to 5 km. The measurement points were selected depending on accessibility, geomorphic expression of the fault trace, and/or natural environmental conditions.

Diffuse CO_2 degassing from soils is commonly fed by different sources, such as biological carbon, hydrothermal carbon, and their mixture[69]. To identify different populations in the soil CO_2 flux data, we followed the statistical method proposed by Sinclair[70]. As shown by examples of soil CO_2 emissions from hydrothermal fields (Supplementary Fig. 4), the background populations of soil CO_2 fluxes (i.e., biogenic CO_2) could be well distinguished from the endogenic populations (i.e., hydrothermal CO_2). Average fluxes with 95% confidence intervals were calculated for the identified populations of hydrothermal fields following ref. 70. (Supplementary Table 3). High flux populations represent CO_2 derived from

endogenic sources, such as those observed in volcanic-hydrothermal systems[69]. Low flux populations refer to CO_2 associated with biological activities in the soils, while intermediate populations are commonly interpreted as a mixture of biogenic and hydrothermal carbon. These average soil CO_2 fluxes ($F_{\text{hf,CO2}}$ in g m^{-2} d^{-1}) were then combined with estimated degassing areas ($S_{\text{hf,degassing}}$ in km^2) to obtain a CO_2 emission ($E_{\text{hf,CO2}}$ in Mt yr^{-1}) for each hydrothermal field and the resulting CO_2 flux were summed together. The diffuse soil CO_2 emissions of 2.04 ± 0.98 Mt yr^{-1} for the hydrothermal fields in the entire TTYR (Supplementary Table 2).

For the profiles of soil CO_2 fluxes without visible hydrothermal manifestations, we classified the soil CO_2 flux data into two groups for southern, central, and northern segments of the TTYR (Supplementary Table 4): (i) background areas with comparable fluxes to biogenic values, and (ii) fault zone with higher average soil CO_2 fluxes (Supplementary Fig. 8). Considering the irregular spacing and sparse sampling used in regional surveys, we adopted the structural-area method proposed by Lee et al. [53] for estimating total CO_2 fluxes from fault zone and background area in the TTYR. To constrain spatial variations in CO_2 emission efficiency, we compared the average soil CO_2 flux of the fault zone profiles and background areas and found that diffuse soil CO_2 emissions are generally in the same magnitude among different segments of the TTYR. Specifically, the average soil CO_2 flux of the fault zone profiles is 36.3, 42.3, and 25 g m^{-2} d^{-1} for the southern, central, and northern segments of the TTYR, and that of the background area is 11, 8.6, and 10.4 g m^{-2} d^{-1} for southern, central and northern TTYR (see details in Supplementary Data 4). Therefore, the average soil CO_2 flux of the fault zones and background areas was multiplied by the area of soil degassing to estimate the corresponding total CO_2 output. The calculated soil CO_2 fluxes from the fault zone and background area were 1.40 ± 0.53 Mt yr^{-1} and 13.9 ± 2.6 Mt yr^{-1}, respectively (Supplementary Table 2). The uncertainty in flux estimates is derived from the standard error of the average soil CO_2 fluxes. Detailed methods for estimation of soil degassing area and flux calculation (including equations and procedures) are provided in Supplementary Information. Finally, it should be emphasized that estimating CO_2 output for a rift such as the TTYR remains challenging, and assuming the measured flux data from a limited study area are representative of the entire rift is feasible at the current stage.

Carbon isotope mass balance models

For free gases from thermal springs, we combined He with C isotope systematics to calculate the proportions of different carbon source components using a ternary mixing model that involves the mantle (MORB), marine carbonate (CAR), and organic sediments (ORG) end-members[31]. Mantle, carbonate, and organic sediments are assumed to have CO_2/^{3}He and $\delta^{13}C_{CO2}$ values of 2×10^9 and $-6.5 \pm 2.5‰$, 1×10^{13} and $0 \pm 2‰$, as well as 1×10^{13} and $-30 \pm 10‰$, respectively (Fig. 2). This model indicates that the fraction of mantle carbon (M) + carbonate (C) is about 75–88%, and organic sediments (S) accounts for the rest fraction of carbon (12–25%; Supplementary Data 1). Notably, it is difficult to constrain the proportion of metamorphic carbon solely based on the model of Sano and Marty[31], because the $\delta^{13}C$ value of metamorphic carbon could be close to that of either inorganic carbon or organic carbon depending on the protoliths of metamorphic decarbonation reactions[71–73].

For diffuse soil CO_2 emissions, the deep CO_2 of hydrothermal origins could migrate toward the surface through the porosity of rocks and fractures/faults, which is expected to mix with CO_2 derived from biogenic sources and the atmosphere. Combined with the evaluation of the area of soil emanation (Supplementary Methods), the CO_2 outgassing fluxes in background areas, fault zones, and hydrothermal fields were estimated to be 13.9 ± 2.60, 1.40 ± 0.53, and 2.04 ± 0.98 Mt yr^{-1}, respectively, including CO_2 from deep and shallow sources. To avoid overestimation of deeply-sourced CO_2 fluxes, we subtracted shallow carbon (e.g., biogenic CO_2) fractions from the total CO_2 output based on a carbon isotope mass balance model based on carbon isotopes ($\delta^{13}C$) and abundances of CO_2 in soil gases (Supplementary Fig. 9). The hydrothermal source is assumed to have 100 vol.% CO_2 and a $\delta^{13}C$ value of $-2‰$ (constrained by a scenario of batch

equilibrium CO_2 degassing from a DIC end-member with $\delta^{13}C$ value of $+2‰$, i.e., equilibrium fractionation value $\Delta^{13}C_{eq} = +4‰$), while the air has 0.04 vol.% CO_2 and a $\delta^{13}C$ value of $-8‰$. For the biogenic CO_2 end-member, we used a $\delta^{13}C$ value ($-23.6‰$) reported for modern soils of the Tibetan Plateau[74] and assumed pure CO_2 production (i.e., 100 vol.% CO_2) for biogenic source components. This ternary mixing model yielded average deep CO_2 proportions of 62% and 33% for soil gas seeping in hydrothermal fields ($f_{hf,deep}$) and fault zones ($f_{fz,deep}$), respectively (Supplementary Data 3). In contrast, deeply-sourced CO_2 was remarkably low (9%) in soils of the background areas ($f_{ba,deep}$). Deep CO_2 fluxes from diffuse soil in the TTYR were calculated by summing the deep CO_2 fluxes of the hydrothermal fields ($E_{hf,CO2} \times f_{hf,deep}$), fault zones ($E_{fz,CO2} \times f_{fz,deep}$), and background areas ($E_{ba,CO2} \times f_{ba,deep}$). The results show that deep CO_2 fluxes of soil seeping in the TTYR are 1.26 ± 0.60 Mt yr^{-1} in hydrothermal fields, 0.46 ± 0.18 Mt yr^{-1} in fault zones, and 1.25 ± 0.23 Mt yr^{-1} in background areas. Taken together, total deep CO_2 output through soils would be 2.97 ± 1.01 Mt yr^{-1} for the TTYR (Supplementary Table 2).

CO_2 flux extrapolation to the extensional tectonics

To extrapolate our measurements to extensional tectonics (mainly rifts and normal faults) of the Himalayan-Tibetan orogen, we compiled basic geological parameters such as the number of hydrothermal fields ($n = \sim650$ in the China part of the Himalayan-Tibetan orogen[13]) and total area of major seven near N-S striking rifts (fault zone = ~545 km^2; background area = $\sim13,563$ km^2) in northern Himalaya and southern Tibet and that of other smaller scale normal faults (~337 km^2) in the same region (Supplementary Table 5). A detailed procedure of the CO_2 flux extrapolation method was given in Supplementary Information. The estimated total deep CO_2 flux is 37 ± 21 Mt yr^{-1} for the rifts and normal faults in the northern Himalaya and southern Tibet. Most of the deep CO_2 output is accounted for by diffuse soil emanations from hydrothermal fields (Supplementary Table 6). Note that rift and normal fault systems in more northerly and easterly tectonic units (e.g., Qiangtang Block and Songpan-Ganzi Block) of the Tibetan Plateau and its surroundings are beyond the scope of this study and are not considered in flux extrapolation also due to the lack of observational data. Therefore, our estimate of deep CO_2 flux represents a conservative value of the entire rifts and normal fault systems of the Himalayan-Tibetan orogen. To reduce the error of deep carbon flux estimates, more work is required to investigate other rifts and normal faults in the Himalayan-Tibetan orogen.

Data availability

All data generated or analyzed in this study are provided in the online version of this article and Supplementary Information. Supplementary Data 1 to 4 (Excel spreadsheets) have been deposited at Zenodo (https://doi.org/10.5281/zenodo.11125483).

References

1. Ding, L. et al. Timing and mechanisms of Tibetan Plateau uplift. *Nat. Rev. Earth Environ.* **3**, 652–667 (2022).
2. Guo, Z., Wilson, M., Dingwell, D. B. & Liu, J. India-Asia collision as a driver of atmospheric CO_2 in the Cenozoic. *Nat. Commun.* **12**, 3891 (2021).
3. Raymo, M. & Ruddiman, W. F. Tectonic forcing of late Cenozoic climate. *Nature* **359**, 117–122 (1992).
4. Hilton, R. G. & West, A. J. Mountains, erosion and the carbon cycle. *Nat. Rev. Earth Environ.* **1**, 284–299 (2020).
5. Märki, L. et al. An unshakable carbon budget for the Himalaya. *Nat. Geosci.* **14**, 745–750 (2021).
6. Jiang, H. et al. Chemical weathering of small catchments on the Southeastern Tibetan Plateau I: water sources, solute sources and weathering rates. *Chem. Geol.* **500**, 159–174 (2018).
7. Kerrick, D. M. & Caldeira, K. Metamorphic CO_2 degassing from orogenic belts. *Chem. Geol.* **145**, 213–232 (1998).
8. Zondervan, J. R. et al. Rock organic carbon oxidation CO_2 release offsets silicate weathering sink. *Nature* **623**, 329–333 (2023).
9. Becker, J. A., Bickle, M. J., Galy, A. & Holland, T. J. B. Himalayan metamorphic CO_2 fluxes: Quantitative constraints from hydrothermal springs. *Earth Planet. Sci. Lett.* **265**, 616–629 (2008).
10. Girault, F. et al. Persistent CO_2 emissions and hydrothermal unrest following the 2015 earthquake in Nepal. *Nat. Commun.* **9**, 2956 (2018).
11. Zhang, L. et al. Flux and genesis of CO_2 degassing from volcanic-geothermal fields of Gulu-Yadong rift in the Lhasa terrane, South Tibet: Constraints on characteristics of deep carbon cycle in the India-Asia continent subduction zone. *J. Asian Earth Sci.* **149**, 110–123 (2017).
12. Zhang, M. et al. Metamorphic CO_2 emissions from the southern Yadong-Gulu rift, Tibetan Plateau: Insights into deep carbon cycle in the India-Asia continental collision zone. *Chem. Geol.* **584**, 120534 (2021).
13. Zhao, W., Guo, Z., Li, J., Ma, L. & Liu, J. Fluxes and genesis of deep carbon emissions from southern Tibetan Plateau and its adjacent regions. *Acta Petrol. Sin.* **38**, 1541–1556 (2022).
14. Zhang, M. et al. Magma-derived CO_2 emissions in the Tengchong volcanic field, SE Tibet: Implications for deep carbon cycle at intra-continent subduction zone. *J. Asian Earth Sci.* **127**, 76–90 (2016).
15. Gaillardet, J. & Galy, A. Himalaya—carbon sink or source? *Science* **320**, 1727–1728 (2008).
16. Tamburello, G., Pondrelli, S., Chiodini, G. & Rouwet, D. Global-scale control of extensional tectonics on CO_2 Earth degassing. *Nat. Commun.* **9**, 4608 (2018).
17. Lee, C.-T., Jiang, H., Dasgupta, R. & Torres, M. A framework for understanding whole-Earth carbon cycling. In *Deep Carbon: Past to Present* (eds. Orcutt, B. N., Daniel, I. & Dasgupta, R.) pp. 313–357 (Cambridge Univ. Press, Cambridge, 2019).
18. Brune, S., Williams, S. E. & Müller, R. D. Potential links between continental rifting, CO_2 degassing and climate change through time. *Nat. Geosci.* **10**, 941–946 (2017).
19. Nábělek, J. et al. Underplating in the Himalaya-Tibet collision zone revealed by the Hi-CLIMB experiment. *Science* **325**, 1371–1374 (2009).
20. Craig, T. J., Copley, A. & Jackson, J. Thermal and tectonic consequences of India underthrusting Tibet. *Earth Planet. Sci. Lett.* **353–354**, 231–239 (2012).
21. Nábělek, P. I. & Nábělek, J. L. Thermal characteristics of the Main Himalaya Thrust and the Indian lower crust with implications for crustal rheology and partial melting in the Himalaya orogen. *Earth Planet. Sci. Lett.* **395**, 116–123 (2014).
22. Kapp, P. & Guynn, J. H. Indian punch rifts Tibet. *Geology* **32**, 993–996 (2004).
23. Yin, A. Cenozoic tectonic evolution of the Himalayan orogen as constrained by along-strike variation of structural geometry, exhumation history, and foreland sedimentation. *Earth Sci. Rev.* **76**, 1–131 (2006).
24. Buttitta, D. et al. Regulation of deep carbon degassing by gas-rock-water interactions in a seismic region of Southern Italy. *Sci. Total Environ.* **897**, 165367 (2023).
25. Gilfillan, S. M. V. et al. Solubility trapping in formation water as dominant CO_2 sink in natural gas fields. *Nature* **458**, 614–618 (2009).
26. Barry, P. H. et al. Volatile sources, sinks and pathways: a helium-carbon isotope study of Baja California fluids and gases. *Chem. Geol.* **550**, 119722 (2020).
27. Zhang, M. et al. Linking deeply-sourced volatile emissions to plateau growth dynamics in southeastern Tibetan Plateau. *Nat. Commun.* **12**, 4157 (2021).
28. Newell, D. L. et al. Aqueous and isotope geochemistry of mineral springs along the southern margin of the Tibetan plateau: Implications

29. Ray, M. C., Hilton, D. R., Muñoz, J., Fischer, T. P. & Shaw, A. M. The effects of volatile recycling, degassing and crustal contamination on the helium and carbon geochemistry of hydrothermal fluids from the Southern Volcanic Zone of Chile. *Chem. Geol.* **266**, 38–49 (2009).

30. O'Nions, R. K. & Oxburgh, E. R. Helium, volatile fluxes and the development of continental crust. *Earth Planet. Sci. Lett.* **90**, 331–347 (1988).

31. Sano, Y. & Marty, B. Origin of carbon in fumarolic gas from island arcs. *Chem. Geol.* **119**, 265–274 (1995).

32. Zhao, D. et al. Hydrogeochemical study of hot springs along the Tingri-Nyima rift: relationship between fluids and earthquakes. *Water* **15**, 1634 (2023).

33. Groppo, C., Rolfo, F. & Frezzotti, M. L. CO_2 outgassing during collisional orogeny is facilitated by the generation of immiscible fluids. *Commun. Earth Environ.* **3**, 13 (2022).

34. Zhang, M., Guo, Z., Zhang, L., Sun, Y. & Cheng, Z. Geochemical constraints on origin of hydrothermal volatiles from southern Tibet and the Himalayas: Understanding the degassing systems in the India-Asia continental subduction zone. *Chem. Geol.* **469**, 19–33 (2017).

35. Yokoyama, T., Nakai, S. & Wakita, H. Helium and carbon isotopic compositions of hot spring gases in the Tibetan Plateau. *J. Volcanol. Geotherm. Res.* **88**, 99–107 (1999).

36. Ballentine, C. J., Burgess, R. & Marty, B. Tracing fluid origin, transport and interaction in the crust. *Rev. Mineral. Geochem.* **47**, 539–614 (2002).

37. Hoke, L., Lamb, S., Hilton, D. R. & Poreda, R. J. Southern limit of mantle-derived geothermal helium emissions in Tibet: Implications for lithospheric structure. *Earth Planet. Sci. Lett.* **180**, 297–308 (2000).

38. Klemperer, S. L. et al. Limited underthrusting of India below Tibet: ^{3}He/^{4}He analysis of thermal springs locates the mantle suture in continental collision. *Proc. Natl. Acad. Sci.* **119**, e2113877119 (2022).

39. Zhao, W. et al. Subducting Indian lithosphere controls the deep carbon emission in Lhasa Terrane, southern Tibet. *J. Geophys. Res.: Solid Earth* **127**, e2022JB024250 (2022).

40. Girault, F. et al. The Syabru-Bensi hydrothermal system in central Nepal: 1. Characterization of carbon dioxide and radon fluxes. *J. Geophys. Res.: Solid Earth* **119**, 4017–4055 (2014).

41. Chen, Y., Li, W., Yuan, X., Badal, J. & Teng, J. Tearing of the Indian lithospheric slab beneath southern Tibet revealed by SKS-wave splitting measurements. *Earth Planet. Sci. Lett.* **413**, 13–24 (2015).

42. Kapp, P. & DeCelles, P. G. Mesozoic–Cenozoic geological evolution of the Himalayan-Tibetan orogen and working tectonic hypotheses. *Am. J. Sci.* **319**, 159–254 (2019).

43. Evans, M. J., Derry, L. A. & France-Lanord, C. Degassing of metamorphic carbon dioxide from the Nepal Himalaya. *Geochem. Geophys. Geosyst.* **9**, Q04021 (2008).

44. Randazzo, P. et al. Active degassing of crustal CO_2 in areas of tectonic collision: a case study from the Pollino and Calabria sectors (Southern Italy). *Front. Earth Sci.* **10**, 946707 (2022).

45. Hodges, K. V. Crustal decoupling in collisional orogenesis: examples from the East Greenland Caledonides and Himalaya. *Annu. Rev. Earth Planet. Sci.* **44**, 685–708 (2016).

46. Furlong, K. P. & Chapman, D. S. Heat flow, heat generation, and the thermal state of the lithosphere. *Annu. Rev. Earth Planet. Sci.* **41**, 385–410 (2013).

47. Jiang, G. et al. Terrestrial heat flow of continental China: updated dataset and tectonic implications. *Tectonophysics* **753**, 36–48 (2019).

48. Ferry, J. M. Regional metamorphism of the Waits River Formation, eastern Vermont: Delineation of a new type of giant metamorphic hydrothermal system. *J. Petrol.* **33**, 45–94 (1992).

49. Unsworth, M. J. et al. Crustal rheology of the Himalaya and Southern Tibet inferred from magnetotelluric data. *Nature* **438**, 78–81 (2005).

50. Wang, J., Wu, F., Zhang, J., khanal, G. & Yang, L. The Himalayan collisional orogeny: a metamorphic perspective. *Acta Geol. Sin.* **96**, 1842–1866 (2022).

51. Cao, H.-W. et al. Himalayan leucogranites: a review of geochemical and isotopic characteristics, timing of formation, genesis, and rare metal mineralization. *Earth Sci. Rev.* **234**, 104229 (2022).

52. Stewart, E. M. et al. Carbonation and decarbonation reactions: Implications for planetary habitability. *Am. Mineral.* **104**, 1369–1380 (2019).

53. Lee, H. et al. Massive and prolonged deep carbon emissions associated with continental rifting. *Nat. Geosci.* **9**, 145–149 (2016).

54. Wolff, R. et al. Rift propagation in south Tibet controlled by underthrusting of India: a case study at the Tangra Yumco graben (south Tibet). *J. Geol. Soc.* **180**, jgs2022–jgs2090 (2023).

55. Zhang, B., Bao, X., Wu, Y., Xu, Y. & Yang, W. Southern Tibetan rifting since late Miocene enabled by basal shear of the underthrusting Indian lithosphere. *Nat. Commun.* **14**, 2565 (2023).

56. Chiodini, G. et al. Correlation between tectonic CO_2 Earth degassing and seismicity is revealed by a 10-year record in the Apennines, Italy. *Sci. Adv.* **6**, eabc2938 (2020).

57. Le Voyer, M. et al. Carbon fluxes and primary magma CO_2 contents along the global mid-ocean ridge system. *Geochem. Geophys. Geosyst.* **20**, 1387–1424 (2019).

58. Bianchi, D. et al. Low helium flux from the mantle inferred from simulations of oceanic helium isotope data. *Earth Planet. Sci. Lett.* **297**, 379–386 (2010).

59. Chiodini, G., Pappalardo, L., Aiuppa, A. & Caliro, S. The geological CO_2 degassing history of a long-lived caldera. *Geology* **43**, 767–770 (2015).

60. Barry, P. H. et al. Forearc carbon sink reduces long-term volatile recycling into the mantle. *Nature* **568**, 487–492 (2019).

61. Marty, B. & Tolstikhin, I. N. CO_2 fluxes from mid-ocean ridges, arcs and plumes. *Chem. Geol.* **145**, 233–248 (1998).

62. Muirhead, J. D. et al. Displaced cratonic mantle concentrates deep carbon during continental rifting. *Nature* **582**, 67–72 (2020).

63. Foley, S. F. & Fischer, T. P. An essential role for continental rifts and lithosphere in the deep carbon cycle. *Nat. Geosci.* **10**, 897–902 (2017).

64. Fischer, T. P. & Aiuppa, A. AGU Centennial Grand Challenge: volcanoes and deep carbon global CO_2 emissions from subaerial volcanism—Recent progress and future challenges. *Geochem. Geophys. Geosyst.* **21**, e2019GC008690 (2020).

65. Plank, T. & Manning, C. E. Subducting carbon. *Nature* **574**, 343–352 (2019).

66. Mason, E., Edmonds, M. & Turchyn, A. V. Remobilization of crustal carbon may dominate volcanic arc emissions. *Science* **357**, 290–294 (2017).

67. Shields, G. A. & Mills, B. J. W. Tectonic controls on the long-term carbon isotope mass balance. *Proc. Natl. Acad. Sci. USA* **114**, 4318–4323 (2017).

68. Chiodini, G., Cioni, R., Guidi, M., Raco, B. & Marini, L. Soil CO_2 flux measurements in volcanic and geothermal areas. *Appl. Geochem.* **13**, 543–552 (1998).

69. Chiodini, G. et al. Carbon isotopic composition of soil CO_2 efflux, a powerful method to discriminate different sources feeding soil CO_2 degassing in volcanic-hydrothermal areas. *Earth Planet. Sci. Lett.* **274**, 372–379 (2008).

70. Sinclair, A. J. Selection of threshold values in geochemical data using probability graphs. *J. Geochem. Explor.* **3**, 129–149 (1974).

71. Cook-Kollars, J., Bebout, G. E., Collins, N. C., Angiboust, S. & Agard, P. Subduction zone metamorphic pathway for deep carbon cycling: I. Evidence from HP/UHP metasedimentary rocks, Italian Alps. *Chem. Geol.* **386**, 31–48 (2014).

72. Zhou, Z., Chu, X., Tang, M. & Leybourne, M. Exploring hindered decarbonation in contact metamorphism: a glimpse into marble aureoles in Southern Tibet. *Earth Planet. Sci. Lett.* **626**, 118519 (2024).

73. Zheng, Y.-F., Fu, B., Gong, B. & Li, L. Stable isotope geochemistry of ultrahigh pressure metamorphic rocks from the Dabie–Sulu orogen in China: implications for geodynamics and fluid regime. *Earth Sci. Rev.* **62**, 105–161 (2003).
74. Lu, H. et al. Distribution of carbon isotope composition of modern soils on the Qinghai-Tibetan Plateau. *Biogeochemistry* **70**, 275–299 (2004).

Acknowledgements

Author contributions

S.X. and M.Z. conceived the idea and led the study. W.L., M.Z., L.C., and X.Z. collected samples and conducted in-situ CO_2 flux observations. W.L. and Y.L. (Yi Liu) prepared and analyzed all samples. W.L., M.Z., and Y.L. (Yi Liu) compiled data, performed geochemical modeling, and calculated CO_2 fluxes. M.Z. and W.L. wrote the manuscript with inputs from S.X., Y.S., X.Z., Y.L. (Ying Li), L.Z., Y.-C.L., and C.-Q.L. All authors contributed to data interpretations and commented on the manuscript.

Competing interests

The authors declare no competing interests.

Additional information

Supplementary information The online version contains supplementary material available at https://doi.org/10.1038/s43247-024-01438-z.

Correspondence and requests for materials should be addressed to Maoliang Zhang or Sheng Xu.

Peer review information *Communications Earth & Environment* thanks the anonymous reviewers for their contribution to the peer review of this work. Primary Handling Editors: Carolina Ortiz Guerrero. A peer review file is available

Reprints and permissions information is available at http://www.nature.com/reprints

Publisher's note Springer Nature remains neutral with regard to jurisdictional claims in published maps and institutional affiliations.